ChemPubSoc Europe

DOI: 10.1002/chem.201800079

CHEMISTRY A European Journal Full Paper

Multicomponent Reactions | *Very Important Paper*

Three-Component Activation/Alkynylation/Cyclocondensation (AACC) Synthesis of Enhanced Emission Solvatochromic 3-Ethynylquinoxalines

Franziska K. Merkt,[a] Simon P. Höwedes,[a] Charlotte F. Gers-Panther,[a] Irina Gruber,[b] Christoph Janiak,[b] and Thomas J. J. Müller*[a]

Abstract: 2-Substituted 3-ethynylquinoxaline chromophores can be readily synthesized by a consecutive activation–alkynylation–cyclocondensation (AACC) one-pot sequence in a three-component manner. In comparison with the previously published four-component glyoxylation starting from electron-rich π-nucleophiles, the direct activation of (hetero)aryl glyoxylic acids allows the introduction of substituents that cannot be directly accessed by glyoxylation. By introducing *N*,*N*-dimethylaniline as a strong donor in the 2-position, the emission solvatochromicity of 3-ethynylquinoxalines can be considerably enhanced to cover the spectral range from blue–green to deep red–orange with a single chromophore in a relatively narrow polarity window. The diversity-oriented nature of the synthetic multicomponent reaction concept enables comprehensive investigations of structure–property relationships by Hammett correlations and Lippert–Mataga analysis, as well as the elucidation of the electronic structure of the emission solvatochromic π-conjugated donor–acceptor systems by DFT and time-dependent DFT calculations with the PBEh1PBE functional for a better reproduction of the dominant charge-transfer character of the longest wavelength absorption band.

Introduction

Tailor-made fluorophores with designed emission characteristics have become increasingly important as functional constituents[1] in materials and life sciences, and their applications are widespread, from organic electronics,[2] such as organic field effect transistors (OFETs), organic light-emitting diodes (OLEDs), and dye-sensitized solar cells (DSSCs),[3] to bioanalytical imaging and sensing,[4] and diagnostics.[5] Fluorophores with color response to the surrounding media are particularly interesting.[6] This phenomenon observable by eye is called solvatochromism,[7] and it directly corresponds to a significant change of the dipole moment upon excitation of the chromophore from S_0 to the vibrationally relaxed S_1 state.[8] As a consequence, a steady demand for novel fluorophore structures and emission profiles poses a major challenge to synthetic chemistry to provide suitable libraries for systematic investigations to establish reliable structure–property correlations of the photophysical behavior. Diversity-oriented synthesis[9] is very advantageous because highly diverse products can be readily obtained by the same reaction principle through variation of suitable starting materials. In particular, multicomponent reactions (MCRs)[10] and one-pot strategies combine beneficial economic and ecological aspects for reaching this challenging goal. In the sense of a chromophore concept—a chromogenic application of the MCR concept—functional chromophores have become accessible more easily and more generally;[11] an approach that has now been systematically extended to a powerful tool in fluorophore design.[12]

Quinoxaline and pyrazine dyes, which can be designed by various strategies,[13] have received considerable attention as prospective and potential electroluminescent materials[14–17] and as functional chromophores in bioanalytics.[18,19] These electron-withdrawing core heterocycles represent a unit of paramount importance for the construction of push–pull systems[20,21] and intramolecular charge-transfer (ICT) complexes.[22] The presence of Brønsted and Lewis basic nitrogen atoms[23] promises emission sensitivity towards changes in the surrounding medium triggered by pH, metal ions, solvent polarity, or biological analytes.[24,25] Apart from their luminescence, they also display pronounced solvatochromic shifts of the emission bands. Solvatochromic quinoxaline-based push–pull systems were employed as emissive probes for the binding-site polarity of bovine serum albumin,[26] for exploring site-dependent fluorescence in HEp-2 cells,[27] and as chromophores for DSSCs.[28] Only recently, we[27,29] and Jiang et al.[30] described

[a] F. K. Merkt, S. P. Höwedes, Dr. C. F. Gers-Panther, Prof. Dr. T. J. J. Müller
Institut für Organische Chemie und Makromolekulare Chemie
Heinrich-Heine-Universität Düsseldorf
Universitätsstraße 1, 40225 Düsseldorf (Germany)
E-mail: ThomasJJ.Mueller@uni-duesseldorf.de

[b] I. Gruber, Prof. Dr. C. Janiak
Institut für Anorganische Chemie und Strukturchemie
Heinrich-Heine-Universität Düsseldorf
Universitätsstraße 1, 40225 Düsseldorf (Germany)

Supporting information and the ORCID number(s) for the author(s) of this article can be found under https://doi.org/10.1002/chem.201800079.

the synthesis of emission-solvatochromic indole-substituted quinoxaline derivatives.

In particular, we employed a glyoxylation–alkynylation–cyclocondensation (GACC) sequence to access 3-ethynylquinoxalines in the sense of a consecutive four-component reaction and, as an extension, including a concluding Michael addition to give a glyoxylation–alkynylation–cyclocondensation–addition (GACCA) sequence for accessing 3-(β-aminovinyl)quinoxalines in the sense of a consecutive five-component reaction (Figure 1).

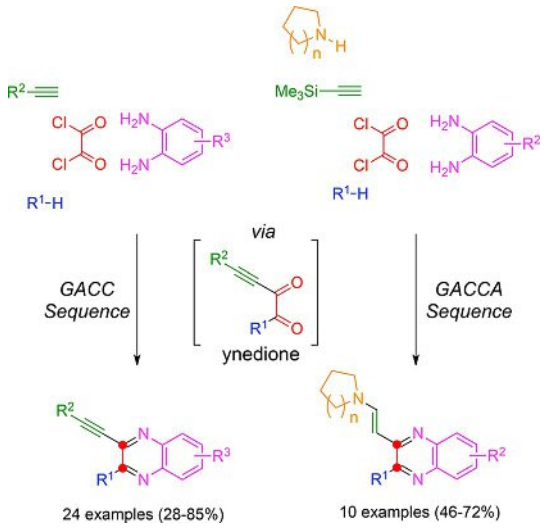

Figure 1. Four-component GACC synthesis of 3-ethynylquinoxalines and five-component GACCA synthesis of 3-(β-aminovinyl)quinoxalines.

The key intermediate is a densely electrophilic ynedione, which is generated through a copper-catalyzed Stephens–Castro alkynylation of the (hetero)aryl glyoxylchloride, formed in a one-pot fashion by glyoxylation of a sufficiently reactive π-nucleophile R¹–H with oxalyl chloride.[31] Alternatively, the (hetero)aryl glyoxylchloride can be generated directly from the (hetero)aryl glyoxylic acid with oxalyl chloride.[32] In contrast to palladium-catalyzed alkynylation, which proceeds with concomitant decarbonylation,[33] the copper-catalyzed variant yields the ynedione. The formation of the common 3-ethynylquinoxaline products or intermediates proceeds through Hinsberg cyclocondensation[34] of the ynedione intermediate with *ortho*-phenylene diamine derivatives.[35]

Although electron-rich π-nucleophiles, in general, are readily employed as substrates in GACC and GACCA sequences, the direct transformation of electroneutral and *para*-substituted benzoid substrates is considerably hampered or impossible. Without doubt, the activation–alkynylation–cyclocondensation (AACC) sequence through the en route generation of (hetero)aryl glyoxylchloride from (hetero)aryl glyoxylic acids and oxalyl chloride[35] offers a viable alternative to access ynediones that has already been employed in a few cases.[24,29]

Herein, we report the improved AACC sequence for synthesizing an expanded series of 2-(hetero)aryl-substituted 3-ethynylquinoxalines in the sense of a consecutive three-component synthesis. In addition, the photophysical properties are systematically studied by absorption and emission spectroscopy, as well as by correlation studies and quantum-chemical calculations.

Results and Discussion

Synthesis and structure

Ynediones are densely functionalized polyelectrophilic functional groups with a powerful synthetic potential that has, however, scarcely been explored so far.[36,37] As already mentioned, electron-rich π-nucleophiles can be successfully employed in the GACC sequence; however, no electron-rich *para*-substituted arenes, carbazole and benzo[*b*]thiophene derivatives, and bromo-substituted thiophenes could be successfully transformed (see Tables S1 and S2 in the Supporting Information). This shortcoming prompted us to directly begin with (hetero)aryl glyoxylic acids as starting materials. This alternative route to (hetero)aryl glyoxylchlorides represents an activation that can also be uneventfully performed in a one-pot fashion. Therefore, under Friedel–Crafts conditions, electron-rich *para*-substituted arenes, carbazole, and benzo[*b*]thiophene derivatives were reacted with a slight excess of ethoxy oxalyl chloride in the presence of Lewis acids, such as aluminum chloride or titanium chloride, to give the ethyl (hetero)aryl glyoxylates. The esters were saponified under alkaline conditions to give the desired (hetero)aryl glyoxylic acids **1** (Scheme 1).[38–41] Very few aryl glyoxylic acids are commercially available.

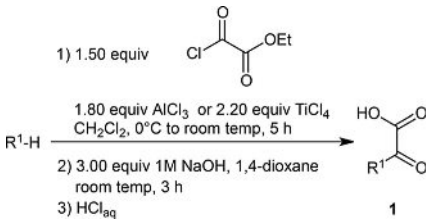

Scheme 1. Synthesis of (hetero)aryl glyoxylic acids **1**.

With (hetero)aryl glyoxylic acids **1** in hand, the consecutive three-component AACC synthesis of 3-ethynylquinoxalines **4** commences with the activation of the (hetero)aryl glyoxylic acids **1** with one equivalent of oxalyl chloride at RT or 50 °C in 1,4-dioxane. The (hetero)aryl glyoxylic chlorides, without isolation, were coupled at RT with terminal alkynes **2** in the presence of a catalytic amount of copper(I) iodide and an equal stoichiometric amount of triethylamine to form the ynediones. Without isolation, the ynediones were directly reacted with the 1,2-diamino derivatives **3** in the presence of acetic acid and methanol to yield 24 examples of 2-(hetero)aryl-substituted 3-ethynylquinoxalines **4** in moderate to very good yields (Scheme 2 and Table 1).

The proposed structures of the 2-(hetero)aryl-substituted 3-ethynylquinoxalines **4** were unambiguously supported with results from ^{1}H and ^{13}C NMR spectroscopy, mass spectrometry, IR

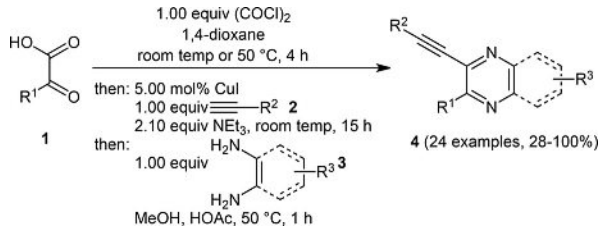

Scheme 2. Consecutive three-component AACC synthesis of 2-(hetero)aryl-substituted 3-ethynylquinoxalines **4**.

spectroscopy, and combustion analysis. Additionally, the structure of compound **4u** was corroborated by X-ray crystal-structure analysis (Figure 2).[42] Compound **4u** crystallizes as yellow needles in the monoclinic space group $P2_1/n$. The 9-phenyl-9*H*-carbazole moiety is twisted out of coplanarity with the 6,7-dichloroquinoxaline core by a dihedral angle of 27°.

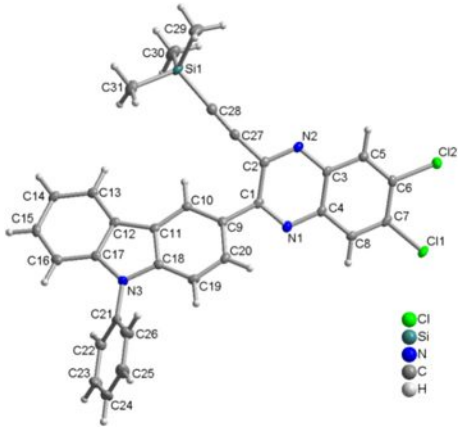

Figure 2. Molecular structure of compound **4u** (thermal ellipsoids shown at the 50% probability level).

Significant π stacking shows rather short centroid–centroid contacts (<3.8 Å), near-parallel ring planes ($\alpha < 10$ to $\approx 0°$ or even exactly 0° by symmetry), small slip angles (β, $\gamma < 25°$), and vertical displacements (slippage <1.5 Å), which translate into a sizable overlap of the aryl-plane areas. (Figure 3).[43,44] The molecules are stacked directly on top of each other, with sizeable π–π stacking along the *b* direction, and they are arranged in undulating layers parallel to the *ac* plane.

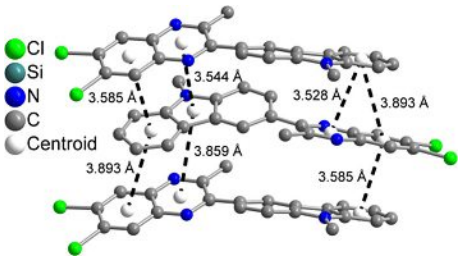

Figure 3. Section of the packing diagram of **4u**, which shows significant π-stacking interactions along the *b* direction (labeled with their centroid–centroid distances; from the trimethylsilylethynyl and phenyl groups, only the ring-bonded atoms have been retained for clarity; for further details, see Table S6 with additional figures in the Supporting Information).

The presented one-pot protocol for the synthesis of 2-(hetero)-aryl-substituted 3-ethynylquinoxalines **4** is particularly interesting because all three reactants, **1**, **2**, and **3**, are employed in strictly equimolar amounts. In addition, upon starting from (hetero)aryl glyoxylic acids **1**, the substituent scope in the title compounds at the 2-position of the quinoxaline core can be considerably expanded, thereby accessing strong and weak donors, as well as electroneutral substitution (Table 1, entries 10–19 and 22–24) and heterocyclic derivatives (Table 1, entries 1–9, 20 and 21); all of these are moieties, the (hetero)-aromatic precursors of which, not transformed in the GACC sequence. The diversity pattern of the alkynes is similar to that in the GACC sequence; however, for the concluding Hinsberg cyclization, a slightly broader substitution pattern can be achieved, in which not only *o*-phenylenediamine (**3a**), 4,5-dichloro-*o*-phenylenediamine (**3b**), and 2,3-diamino-naphthalene (**3c**) are accepted as substrates, but also less reactive 1,2-amino derivatives 4,5-diaminophthalonitrile (**3d**) and diaminomaleonitrile (**3e**) are successfully employed with slightly longer reaction times in the terminal step. Thereby, the diacceptor-enhanced quinoxaline **4r** (Table 1, entry 18) can be accessed, as well as the pyrazine analogue **4s** (Table 1, entry 19).

Photophysical properties

In previous studies on donor-substituted quinoxalines, significantly redshifted emission maxima and large Stokes shifts have been reported.[24,25,45] With the library of 2-(hetero)aryl-substituted 3-ethynylquinoxalines **4** in hand, systematic investigations of the distinct substituent effects on the optical properties were carried out through quantitative absorption and emission spectroscopy (Table 2). The relative fluorescence quantum yields, Φ_F, were determined with suitable standards according to procedures reported in the literature.[46]

In the UV/Vis absorption spectra, two to four distinct broad structureless maxima are found and the longest wavelength bands, $\lambda_{max,abs}$, appear between $\lambda = 352$ and 484 nm, with molar absorption coefficients, ε, ranging from 8100 to 29800 $L\,mol^{-1}\,cm^{-1}$. The remote R^2 substituent at the *para* position of the arylethynyl moiety only has a minor effect on the energy of this absorption and varies from $\lambda = 421$ nm for *N*,*N*-dimethylaniline (Table 2, entry 24) to $\lambda = 417$ nm for phenyl (Table 2, entry 22).

In the spectra of the consanguineous series of the 2-(*p*-*N*,*N*-dimethylanilino)-3-(trimethylsilylethynyl)-substituted quinoxalines **4o–r**, it can be clearly seen that the redshift of the longest wavelength absorption band directly correlates with the increasing electron-withdrawing power of the quinoxaline moiety in the order depicted in Figure 4. This effect, as expected, relies on the acceptor character of the substituents and extension of the π-electron delocalization, as shown by benzoanellation for compound **4q**, in comparison with the mother system **4o**. It is noteworthy to mention that the same qualitative trend is found in the other consanguineous triads **4a–c** and **4f–h** (Table 2, entries 1–3 and 6–8).

Table 1. Consecutive three-component synthesis of 2-(hetero)aryl-substituted 3-ethynylquinoxalines **4**.

Entry	Glyoxylic acid **1**	Alkyne **2**	1,2-Diamino derivative **3**	2-(Hetero)aryl-substituted 3-ethynylquinoxaline **4** (yield [%])[a]
1	2-bromothiophene glyoxylic acid (**1a**)	triisopropylsilylacetylene (**2a**)	*o*-phenylenediamine (**3a**)	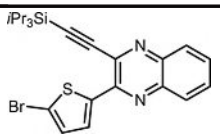 **4a** (91)
2	**1a**	**2a**	4,5-dichloro-*o*-phenylenediamine (**3b**)	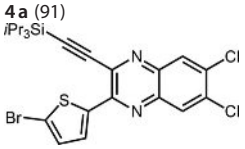 **4b** (69)
3	**1a**	**2a**	2,3-diaminonaphthalene (**3c**)	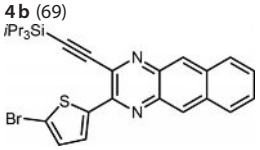 **4c** (74)
4	**1a**	trimethylsilylacetylene (**2b**)	**3a**	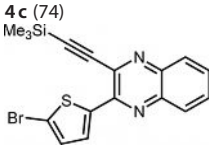 **4d** (78)
5	3-bromothiophene glyoxylic acid (**1b**)	**2a**	**3a**	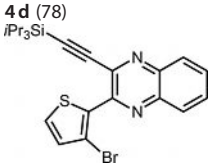 **4e** (31)
6	2-thiophene glyoxylic acid (**1c**)	**2b**	**3a**	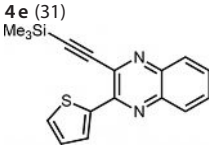 **4f** (88)
7	**1c**	**2b**	**3b**	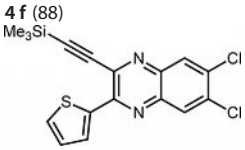 **4g** (67)
8	**1c**	**2b**	**3c**	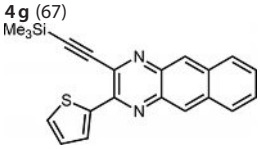 **4h** (86)
9	benzo[*b*]thiophene-glyoxylic acid (**1d**)	**2b**	**3a**	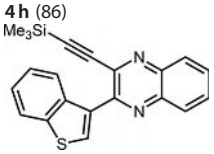 **4i** (43)
10	phenyl glyoxylic acid (**1e**)	**2b**	**3a**	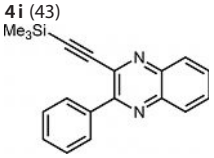 **4j** (85)[b]

Table 1. (Continued)

Entry	Glyoxylic acid **1**	Alkyne **2**	1,2-Diamino derivative **3**	2-(Hetero)aryl-substituted 3-ethynylquinoxaline **4** (yield [%])[a]
11	4-methylphenyl-glyoxylic acid (**1 f**)	**2 b**	**3 a**	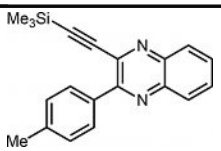 **4 k** (58)
12	4-*tert*-butylphenyl-glyoxylic acid (**1 g**)	**2 b**	**3 a**	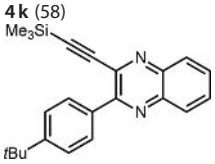 **4 l** (82)
13	4-(methylthio)phenyl-glyoxylic acid (**1 h**)	**2 b**	**3 a**	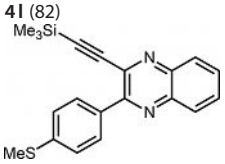 **4 m** (46)
14	4-methoxyphenyl-glyoxylic acid (**1 i**)	**2 b**	**3 a**	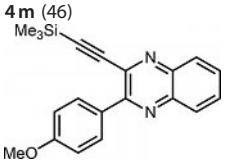 **4 n** (55)
15	4-(dimethylamino)-phenylglyoxylic acid (**1 j**)	**2 b**	**3 a**	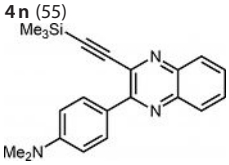 **4 o** (42 %)
16	**1 j**	**2 b**	**3 b**	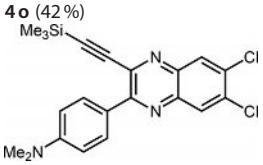 **4 p** (35)
17	**1 j**	**2 b**	**3 c**	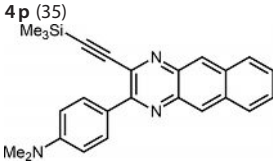 **4 q** (46)
18	**1 j**	**2 b**	4,5-diamino-phthalonitrile (**3 d**)	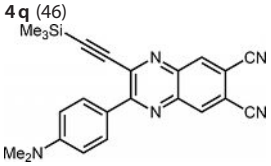 **4 r** (30)
19	**1 j**	**2 b**	diaminomaleo-nitrile (**3 e**)	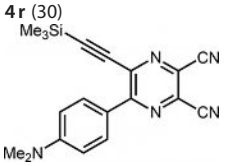 **4 s** (48)

Table 1. (Continued)

Entry	Glyoxylic acid **1**	Alkyne **2**	1,2-Diamino derivative **3**	2-(Hetero)aryl-substituted 3-ethynylquinoxaline **4** (yield [%])[a]
20	4-(9*H*-carbazol-9-yl)-phenylglyoxylic acid (**1k**)	**2b**	**3a**	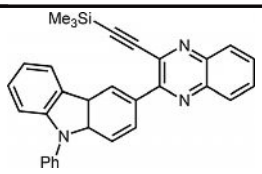 **4t** (87)
21	**1k**	**2b**	**3b**	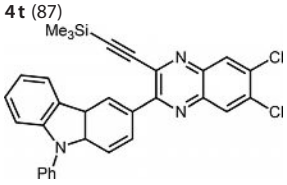 **4u** (100)
22	**1j**	phenyl-acetylene (**2c**)	**3a**	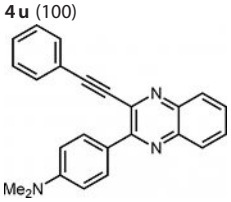 **4v** (53)
23	**1j**	4-methoxyphenyl-acetylene (**2d**)	**3a**	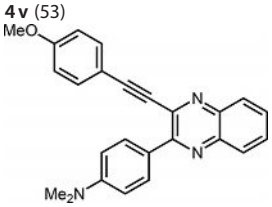 **4w** (60)
24	**1j**	4-dimethylamino-phenylacetylene (**2e**)	**3a**	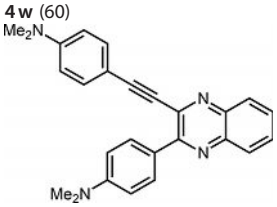 **4x** (28)

[a] Yields after chromatography on silica gel. [b] Synthesized according to ref. [29].

All compounds **4** are intensively luminescent in solutions in dichloromethane with relatively high quantum yields, up to 0.89, with Stokes shifts in the range from 3200 to 8400 cm^{-1}. Generally, the Stokes shifts are significantly larger for the *p*-dimethylamino substituent, which is the strongest donor in the series of compounds **4**, than those for other substituents. In

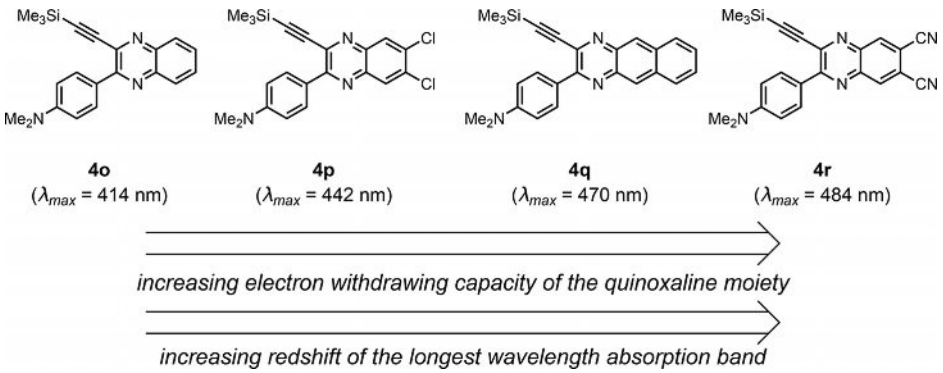

Figure 4. Qualitative effect of the electron-withdrawing capacity of the quinoxaline core on the absorption properties in the series of 2-(*p*-*N*,*N*-dimethylanilino)-3-(trimethylsilylethynyl)-substituted quinoxalines **4o**–**r**.

Table 2. Selected photophysical properties of 2-(hetero)aryl-substituted 3-ethynylquinoxalines **4** (recorded in CH_2Cl_2 at $T = 293$ K).

Entry	Compound	$\lambda_{max,abs}$ [nm][a] (ε [L mol^{-1} cm^{-1}])	$\lambda_{max,em}$ [nm][b] (Φ_F [a.u.])	Stokes shift $\Delta\tilde{\nu}$ [cm^{-1}][c]
1	**4a**	269.0 (21700), 309.0 (28500), 383.0 (12600)	458.0 (0.19)[d]	4300
2	**4b**	271.5 (34500), 313.0 (12400), 394.5 (15900), 406.0 (15400)	463.0 (0.89)[e]	3000
3	**4c**	300.0 (46000), 344.0 (39800), 409.0 (13000)	519.0 (0.76)[e]	5200
4	**4d**	265.0 (22600), 309.0 (31300), 384.0 (12700)	448.0 (0.16)[d]	3700
5	**4e**	267.0 (39400), 355.0 (10400)	423.0 (0.04)[d]	4500
6	**4f**	265.0 (33000), 377.5 (10900)	430.0 (<0.01)[d]	3200
7	**4g**	270.0 (34800), 293.0 (21800sh), 376.0 (11790), 392.0 (13400)	456.0 (<0.01)[d]	4700
8	**4h**	256.0 (27600sh), 296.5 (40000), 337.5 (30600), 413.0 (9414)	522.0 (0.49)[e]	3600
9	**4i**	264.0 (46800), 303.0 (13700), 371.0 (8100)	458.0 (0.01)[d]	5100
10	**4j**	262.5 (45600), 352.0 (10500)	403.0 (<0.01)[d]	3600
11	**4k**	262.0 (48300), 357.0 (10300)	407.0 (<0.01)[d]	3500
12	**4l**	262.0 (12000), 357.0 (11300)	411.0 (<0.01)[d]	3700
13	**4m**	264.0 (22900), 298.5 (48600), 371.5 (12500)	479.0 (0.07)[d]	6000
14	**4n**	262.0 (54800), 284.0 (24300sh), 368.0 (12100)	444.0 (0.50)[d]	4700
15	**4o**	263.0 (35300), 320.0 (24500), 346.0 (16700sh), 414.0 (9000)	598.0 (0.08)[f]	7400
16	**4p**	250.0 (34500), 333.0 (24000), 360.0 (16700sh), 442.0 (9100)	640.0 (0.07)[f]	7000
17	**4q**	298.0 (39400), 328.0 (25600sh), 424.5 (11000), 470.0 (8100)	659.0 (0.03)[f]	8400
18	**4r**	269.0 (32300), 344.5 (10800), 404.0 (15300), 484.0 (9400)	–[g]	–
19	**4s**	279.0 (20500), 305.0 (20300sh), 452.5 (29800)	–[g]	–
20	**4t**	263.0 (56300), 295.0 (39200), 390.0 (11400)	509.0 (0.38)[e]	5100
21	**4u**	268.0 (43400), 296.0 (29200), 408.0 (11000)	535.0 (0.43)[e]	5800
22	**4v**	265.0 (23500), 279.0 (48700sh), 333.0 (49300), 417.0 (16900)	596.0 (0.23)[f]	7200
23	**4w**	267.0 (44600sh), 310.0 (47900sh), 414.0 (18700)	586.0 (0.42)[d]	7100
24	**4x**	299.0 (58500), 329.0 (57900), 421.0 (22300)	574.0 (0.37)[f]	6400

[a] Recorded in CH_2Cl_2, $c(\mathbf{4}) = 10^{-5}$ M at $T = 293$ K. [b] Recorded in CH_2Cl_2 at RT, relative quantum yields were determined by employing procedures reported in the literature (±10%).[46] [c] $\Delta\tilde{\nu} = 1/\lambda_{max,abs} - 1/\lambda_{max,em}$. [d] Recorded at $\lambda_{ex} = 350$ nm, $c(\mathbf{4}) = 10^{-7}$ M, determined with 9,10-diphenylanthracene (DPA) as a standard in cyclohexane ($\Phi_F = 1.00$). [e] Recorded at $\lambda_{ex} = 420$ nm, $c(\mathbf{4}) = 10^{-7}$ M, determined with coumarin 153 as a standard in MeOH ($\Phi_F = 0.45$). [f] Recorded at $\lambda_{ex} = 430$ nm, $c(\mathbf{4}) = 10^{-7}$ M, determined with 4-(dicyanomethylene)-2-methyl-6-(*p*-dimethylaminostyryl)-4*H*-pyran (DCM) in MeOH ($\Phi_F = 0.43$). [g] No signal was detected in CH_2Cl_2.

the consanguineous series of compounds **4j–o** (Figure 5), the increase in Stokes shifts clearly correlates with the donor capacities (see also Figure 4). Interestingly, upon enhancing the push–pull nature going to the extremes of strong donors and strong acceptors, as for the chromophores **4r** and **4s**, the emission in dichloromethane vanishes completely. According to the energy gap law,[47] through which the nonradiative decay of the excited state directly correlates with the redshift of the emission bands, this observation can be additionally supported by the occurrence of fluorescence of these compounds in less polar solvents (*n*-pentane, cyclohexane, toluene).

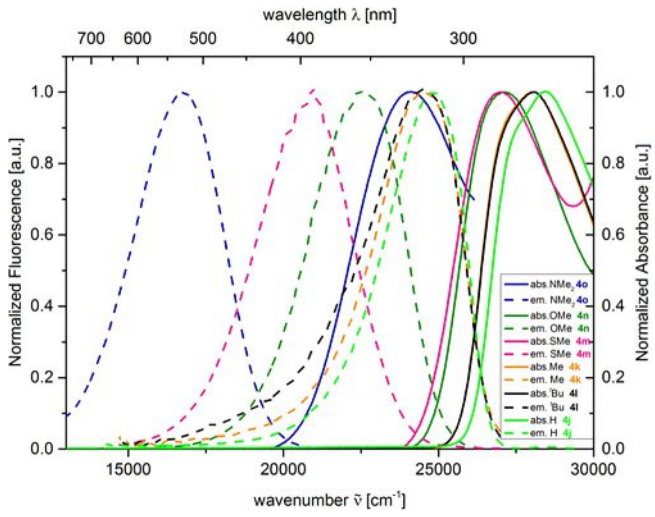

Figure 5. Normalized UV/Vis absorption (recorded in CH_2Cl_2, $T = 293$ K, $c(\mathbf{4}) = 10^{-5}$ M, bold line) and emission bands (recorded in CH_2Cl_2, $T = 293$ K, $c(\mathbf{4}) = 10^{-7}$ M, $\lambda_{ex} = 430$ nm (**4o**), $\lambda_{ex} = 350$ nm (**4j–n**„ dashed line) of the series **4j–o**.

For scrutinizing subtle polar electronic substituent effects in the electronic ground and excited state, the longest wavelength absorption bands, $\lambda_{max,abs}$; emission bands, $\lambda_{max,em}$; and the Stokes shifts, $\Delta\tilde{\nu}$, of the consanguineous series of compounds **4j–o** were correlated with Hammett parameters[48] σ_p, σ_I, σ_R, σ_{p+}, and σ_{p-} to establish linear structure–property relationships. In this series, the best correlations were found for the correlations with parameter σ_{p+}, which accounted for substantial involvement of the stabilization of positive charge upon excitation from the ground state ($\lambda_{max,abs} = 2546.7\,\sigma_{p+} + 28661$ [cm^{-1}]; $r^2 = 0.9635$; Figure 6), emission from a polar vibrationally relaxed excited singlet state ($\lambda_{max,em} = 5204\,\sigma_{p+} + 25588$ [cm^{-1}]; $r^2 = 0.9135$), and a pronounced degree of positive emission solvatochromicity, as reflected by the negative slope of the correlation of the Stokes shifts ($\Delta\tilde{\nu} = -2658\,\sigma_{p+} + 3073$ [cm^{-1}]; $r^2 = 0.8038$; for details on the failed correlations, see Figures S1–S5 in the Supporting Information). The considerably larger slope of the emission correlation compared with the absorption correlation particularly underlines the very polar nature of the vibrationally relaxed excited state, stem-

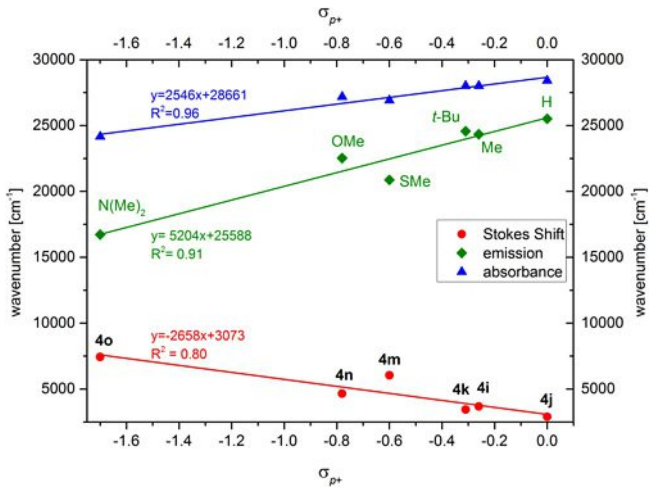

Figure 6. Linear correlation plots of the absorption ($\lambda_{max,abs}$), emission maxima ($\lambda_{max,em}$), and Stokes shifts ($\Delta\tilde{\nu}$) [cm^{-1}] of 3-ethynylquinoxalines **4j–o** against the Hammett parameters, σ_{p+}.

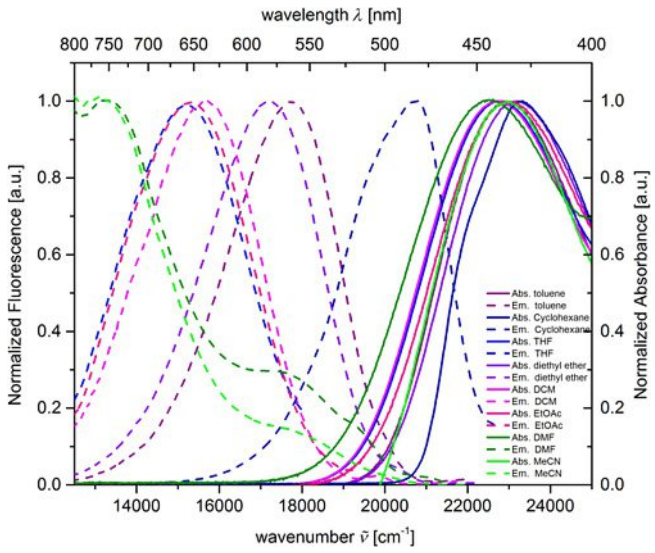

Figure 8. UV/Vis absorption (solid lines) and emission spectra (dashed lines) of compound **4p** measured in eight solvents of different polarity (recorded at $T = 293$ K).

ming from a significant charge-transfer character of the S_1 state. Because the σ parameters of the methylthio substituent (compound **4m**) clearly overestimate stabilizations of discrete positive charges, resonance contributions and combinations of inductive and resonance effects the correlations of $\lambda_{max,abs}$, $\lambda_{max,em}$, and $\Delta\tilde{\nu}$ with σ_p, σ_R, and σ_{p+} of the consanguineous series of compounds **4j–o** without compound **4m** give excellent correlations for σ_p and σ_{p+} parameters (see the Supporting Information for details), it can be concluded that the remote substituent effect is transferred by both inductive and resonance mechanisms involving considerable charge-transfer character.

The first series of 3-ethynylquinoxalines, with moderately electron-releasing indole donors, already showed a pronounced emission solvatochromicity.[29] Upon enhancing the donor capacity in this second series of 3-ethynylquinoxalines **4**, this effect is even more intense for *N*,*N*-dimethylaminophenyl derivatives, covering a broad part of the spectral range upon variation of the solvent polarity from *n*-pentane to acetonitrile (Figures 7 and 8). In this respect, compound **4p** was quantitatively studied by absorption and emission spectroscopy in solvents of different polarity. The absorption solvatochromicity is only minor and ranges between 430 and 447 nm, whereas with increasing solvent polarity the emission maximum, $\lambda_{max,em}$, is shifted bathochromically, ranging from greenish-blue luminescence (478 nm) in cyclohexane to red fluorescence in *N*,*N*-dimethylformamide (755 nm; for detailed data, see Table S4 in the Supporting Information). A change in the dipole moment of the fluorophore upon excitation and dipolar relaxation of the surrounding molecules is the origin of the observed emission solvatochromicity.[49] This phenomenon is rationalized by several theoretical descriptions, including the Lippert–Mataga model, which allows for a quantitative treatment.[50]

Figure 7. Fluorescence of compound **4p** with variable solvent polarity (from left to right: *n*-pentane, cyclohexane, toluene, 1,4-dioxane, diethyl ether, ethyl acetate, dichloromethane, *N*,*N*-dimethyl formamide, acetonitrile; $\lambda_{ex} = 365$ nm, handheld UV lamp).

Therefore, for compound **4p**, the solvatochromicity was evaluated by determining the Lippert–Mataga orientation polarizability [Δf; Eq. (1)] for an extended set of solvents with variable polarity. Consequently, the Stokes shifts ($\Delta\tilde{\nu}$) were plotted against the Δf values, which can be calculated according to Equation (1):

$$\Delta f = \frac{\varepsilon_r - 1}{2\varepsilon_r + 1} - \frac{n^2 - 1}{2n^2 + 1} \quad (1)$$

from the relative permittivity, ε_r, and optical refractive index, n, of the respective solvent.[49]

The Stokes shift, $\Delta\tilde{\nu}$, correlates linearly with the Lippert–Mataga polarity parameters, Δf (ε_r,n), with an excellent goodness of fit ($r^2 = 0.98$; Figure 9); this indicates the dominant importance of a general solvent effect. The change in dipole moment from the electronic ground to the vibrationally relaxed excited state can be calculated according to the Lippert–Mataga equation [Eq. (2)].

$$\tilde{\nu}_a - \tilde{\nu}_f = \frac{2\Delta f}{hca^3}(\mu_E - \mu_G)^2 + const \quad (2)$$

$\Delta\tilde{\nu}_a$ and $\Delta\tilde{\nu}_f$ represent the absorption and emission maxima (in m^{-1}), whereas μ_E and μ_G are the dipole moments in the excited and ground state (in Cm), respectively; ε_0 (8.8542×

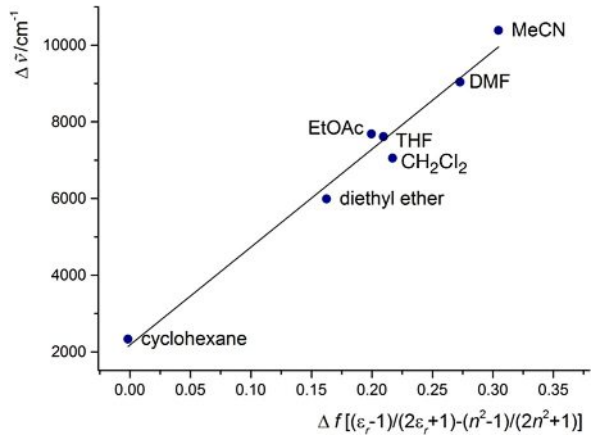

Figure 9. Lippert plot for compound **4p** ($n=7$, $r^2=0.98$).

10^{-12} As V^{-1} m^{-1}) is the vacuum permittivity constant; h (6.6256×10^{-34} J s) is the Planck constant; c (2.9979×10^{8} ms^{-1}) is the speed of light; and a is the radius of the solvent cavity occupied by the molecule (in m).

Assuming a spherical dipole, the Onsager radius, a, which is used to approximate the molecular volume of the molecule in solution, was estimated from the optimized ground-state structure of compound **4p** obtained from DFT calculations (see below). By employing a value of 12.9 Å (12.9×10^{-10} m), the change in dipole moment, $\Delta\mu$, was calculated to be 26 D (8.67×10^{-29} Cm). This large value corresponds to a pronounced charge separation upon charge-transfer excitation.

Calculated electronic structure

A thorough understanding of the photophysical behavior of the consanguineous series of quinoxalines **4o–r** was sought to elucidate the electronic structure by calculating UV/Vis absorption spectra at the DFT level of theory, with a special focus on the comparison of the respective quinoxaline core. The geometries of the electronic ground-state structures were optimized by using Gaussian 09,[51] with the PBEh1PBE functional[52] and the Pople 6-31G(d) basis set.[53] Because the absorption properties were measured in dichloromethane, the polarizable continuum model (PCM) with dichloromethane as a solvent was utilized.[54] All minimum structures were unambiguously assigned by analytical frequency analysis. The structures were chosen as a series of compounds with four different quinoxaline cores from electron-neutral (**4o** and **4q**) to -withdrawing (**4p** and **4r**) properties. The calculated equilibrium ground-state structures show that the *p*-dimethylamino substituent adopts angles between 26 and 38° (for details on the torsion angles of the computed structures **4o–r**, see the Supporting Information). Based upon these optimized ground-state geometries, the electronic transitions S_1 to S_4 were calculated at the time-dependent (TD) DFT level of theory (Table 3). The longest wavelength absorption bands are clearly dominated by HOMO–LUMO transitions, which correctly reproduce the experimentally obtained data.

A closer inspection of the coefficient densities in the Kohn–Sham frontier molecular orbitals (FMOs) of **4o–r** reveals that the HOMO coefficient densities are predominantly localized on the *p*-dimethylamino substituent, whereas much lower coefficient densities are found on the quinoxaline cores (Figure 10). The inverse distribution is observed for the coefficient densities of the LUMOs, which are primarily located on the electron-accepting 3-ethynylquinoxaline cores. Significant FMO coefficients on the quinoxaline moieties are in good agreement with substantial overlap for the Franck–Condon transitions, resulting in pronounced transition dipole moments and oscillator strengths. In addition, the FMO consideration also supports the high degree of charge-transfer π–π* character of the longest wavelength absorption bands. Concurrently, this interpretation is in good agreement with the experimentally observed

Table 3. TD-DFT calculations (PBEh1PBE/6-31G(d)) of the UV/Vis absorption maxima of **4o–r** by applying PCM with dichloromethane as the solvent.

	$\lambda_{max,abs}$ [nm] (ε [L mol^{-1} cm^{-1}])[a]	$\lambda_{max,calcd}$ [nm]	Most dominant contributions	Oscillator strength
4o	414.0 (9000)	424	HOMO→LUMO (98%)	0.103
	346.0 (16700sh)	331	HOMO→LUMO+1 (90%)	0.380
	320.0 (24500)	303	HOMO-1→LUMO (79%) HOMO→LUMO+1 (7%)	0.390
	263.0 (35300)	265	HOMO-1→LUMO+1 (63%) HOMO-6→LUMO+1 (8%) HOMO-3→LUMO+1 (8%)	0.577
4p	442.0 (9100)	457	HOMO→LUMO (98%)	0.140
	360.0 (16700sh)	347	HOMO→LUMO+2 (87%)	0.404
	333.0 (24000)	319	HOMO-1→LUMO (79%) HOMO→LUMO+2 (6%) HOMO-2→LUMO (6%)	0.468
	250.0 (34500sh)	265	HOMO→LUMO+3 (52%) HOMO→LUMO+4 (26%) HOMO→LUMO+6 (12%)	0.087
4q	470.0 (8100)	475	HOMO→LUMO (98%)	0.135
	424.5 (11000)	403	HOMO-1→LUMO (90%) HOMO-3→LUMO (6%)	0.085
	328.0 (25600sh)	322	HOMO→LUMO+1 (58%) HOMO-2→LUMO (20%) HOMO-1→LUMO+1 (18%) HOMO-1→LUMO+1 (32%)	0.669
	298.0 (39400)	285	HOMO→LUMO+2 (26%) HOMO-2→LUMO (16%) HOMO-5→LUMO (11%)	0.789
4r	484.0 (9400)	494	HOMO→LUMO (98%)	0.118
	404.0 (15300)	390	HOMO→LUMO+1 (95%)	0.489
	344.5 (10800)	323	HOMO-1→LUMO (65%) HOMO-2→LUMO (9%)	0.246
	269.0 (32300)	277	HOMO-2→LUMO+1 (63%) HOMO→LUMO+4 (16%)	0.003

[a] Recorded in dichloromethane, $T=293$ K, c(**4o–s**)$=10^{-5}$ M.

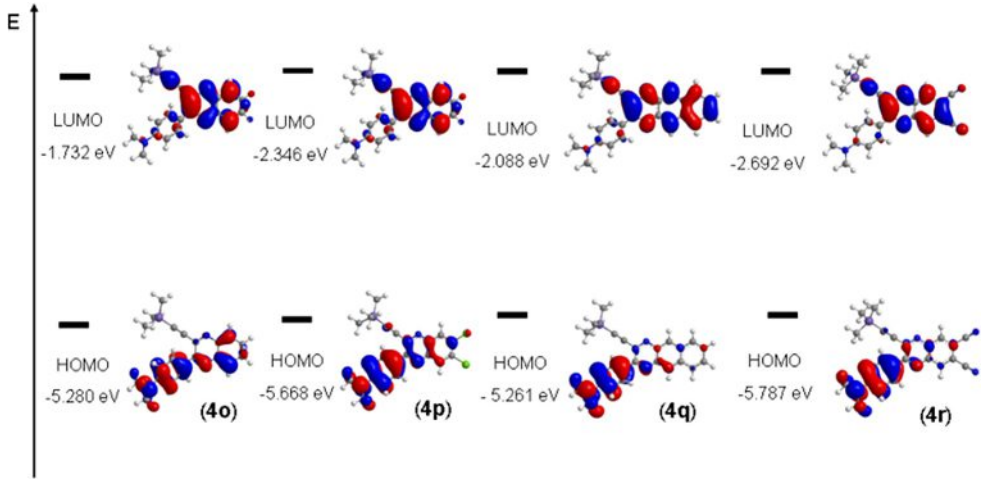

Figure 10. Selected DFT-computed (PBEh1PBE/6-31G(d)) Kohn–Sham FMOs for **4o–r**.

large solvatochromicity of compound **4p**, which is supported by the experimentally determined considerable change in dipole moment upon excitation to the vibrationally relaxed S_1 state that possesses a highly dominant charge-transfer character.

Conclusion

We have successfully synthesized a series of diversity-oriented 2-substituted 3-ethynylquinoxaline chromophores by applying the consecutive three-component AACC protocol. Thereby, 2-substituents at the quinoxaline core can be readily introduced that are either very difficult or impossible to introduce by our previous GACC approach. A series of donor–acceptor conjugates become accessible, in particular, by placing the *p*-dimethylamino substituent as a strong donor. As a result, the positive emission solvochromicity is considerably enhanced in comparison to the first generation of 3-ethynylquinoxalines; this causes a shift of the emission color over a broad part of the spectral range by variation of the solvent polarity. The highly polar nature of the excited state is experimentally elucidated by linear structure–property relationships of the Hammett σ_{p+} parameters with the absorption and emission bands and the Stokes shifts, as well as by Lippert–Mataga determination of the change of dipole moment upon photonic excitation. In addition, the photophysical behavior is supported by DFT and TD-DFT calculations, employing the PBEh1PBE functional, which better reproduces the charge-transfer character of the longest wavelength absorption bands. These emission solvatochromic dyes with enhanced donor capacity are particularly well suited as highly sensitive polarity sensors. Studies to increase the substituent diversity on quinoxaline acceptors by multicomponent strategies and the modulation of the polar excited states by variation of the employed donor and acceptor moieties are currently underway.

Experimental Section

Typical procedure for the three-component synthesis of 4f

Glyoxylic acid **1c** (314 mg, 2.00 mmol) was placed in dry 1,4-dioxane (5 mL) under an argon atmosphere in a sintered screw-cap Schlenk tube, and the solution was then degassed with argon (5 min). The mixture was stirred at RT (water bath) for 5 min. Then, oxalyl chloride (0.18 mL, 2.00 mmol, 1.0 equiv) was added dropwise to the reaction mixture. Thereafter, the mixture was stirred at RT (water bath) for 4 h. Then the mixture was cooled to RT (water bath) for 5 min. Then, CuI (20 mg, 0.10 mmol, 5.00 mol%), **2b** (0.28 mL, 2.00 equiv), and dry triethylamine (0.59 mL, 4.20 mmol) were successively added to the reaction mixture, and stirring at RT was continued for 16 h. Then, methanol (2 mL), **3a** (216 mg, 2.00 mmol), and acetic acid (0.24 mL, 4.00 mmol) were added successively to the reaction mixture. The mixture was stirred at 50 °C for 1 h, water (10 mL) was added, and the aqueous phase was extracted with dichloromethane (3×5 mL/10 mL, monitored by TLC). The combined organic layers were dried (anhydrous sodium sulfate) and the solvents were removed in vacuo. The residue was absorbed onto Celite® and purified by flash chromatography on silica gel (petroleum ether (boiling range 40–60 °C)/ethyl acetate) to give **4f** as a yellow solid (540 mg, 88%; with 314 mg (2.00 mmol) of **1c**). R_f = 0.22 (petroleum ether/ethyl acetate 25:1); m.p. 93 °C; IR: $\tilde{\nu}$ = 3125 (w), 3102 (w), 3065 (w), 2957 (w), 2922 (w), 2901 (w), 2855 (w), 2164 (w), 1558 (w), 1526 (w), 1472 (w), 1460 (w), 1427 (m), 1393 (w), 1362 (w), 1335 (m), 1315 (w), 1300 (w), 1248 (m), 1231 (m), 1219 (m), 1179 (m), 1134 (m), 1119 (w), 1082 (w), 1059 (w), 947 (w), 912 (w), 843 (s), 810 (m), 799 (w), 760 (s), 739 (m), 708 (s), 662 (m), 631 (m), 617 cm^{-1} (m); ^{1}H NMR ($CDCl_3$, 300 MHz): δ = 0.37 (s, 9H), 7.18 (dd, J = 5.1, 3.9 Hz, 1H), 7.57 (dd, J = 5.1, 1.1 Hz, 1H), 7.66–7.78 (m, 2H), 7.99–8.09 (m, 2H), 8.56 ppm (dd, J = 3.9, J = 1.1 Hz, 1H); ^{13}C NMR ($CDCl_3$, 75 MHz): δ = −0.44 (CH_3), 102.8 (C_{quat}), 103.2 (C_{quat}), 127.9 (CH), 128.8 (CH), 128.9 (CH), 130.0 (CH), 130.3 (CH), 130.5 (CH), 131.1 (CH), 134.9 (C_{quat}), 140.4 (C_{quat}), 140.7 (C_{quat}), 141.9 (C_{quat}), 147.7 ppm (C_{quat}); EI-MS: *m/z* (%): 309 (15), 308 (58) $[M]^+$, 307 (33), 295 (10), 294 (24) $[M-CH_3]^+$, 295 (100) $[M-CH_3]^+$, 277 (9) $[M-(CH_3)_2]^+$, 263 (19) $[M-(CH_3)_3]^+$; elemental analysis calcd (%) for $C_{17}H_{16}N_2SSi$ (308.1): C 66.19, H 5.23, N 9.08, S 10.39; found: C 66.46, H 5.33, N 8.78, S 10.12..

Typical procedure for the three-component synthesis of 4p

Glyoxylic acid **1j** (386 mg, 2.00 mmol) was placed in dry 1,4-dioxane (5 mL) under an argon atmosphere in a sintered screw-cap Schlenk tube and the solution was then degassed with argon (5 min). The mixture was stirred at RT (water bath) for 5 min. Then, oxalyl chloride (0.18 mL, 2.00 mmol, 1.0 equiv or 0.09 mL for 1.00 mmol) was added dropwise to the reaction mixture.

Thereafter, the mixture was stirred at 50 °C (oil bath) or room temp. for 4 h. Then the mixture was cooled to RT (water bath) for 5 min. Then, CuI (20 mg, 0.10 mmol, 5.00 mol%), **2b** (0.28 mL, 2.00 equiv), and dry triethylamine (0.59 mL for 2.00 mmol, 4.20 mmol, 2.10 equiv) were successively added to the reaction mixture, and stirring at RT was continued for 16 h. Then, methanol (2 mL), **3b** (361 mg, 2.00 mmol), and acetic acid (0.24 mL, 4.00 mmol) were added successively to the reaction mixture. The mixture was stirred at 50 °C for 1 h, water (10 mL) was added, and the aqueous phase was extracted with dichloromethane (3×5 mL/10 mL, monitored by TLC). The combined organic layers were dried (anhydrous sodium sulfate) and the solvents were removed in vacuo. The residue was absorbed onto Celite® and purified by flash chromatography on silica gel (petroleum ether (boiling range 40–60 °C)/ethyl acetate) to give **4p** as an orange solid (241 mg, 35%). R_f = 0.10 (petroleum ether/ethyl acetate 6:1); m.p. 186 °C; IR: $\tilde{\nu}$ = 3107 (w), 3086 (w), 2955 (w), 2897 (w), 2866 (w), 2824 (w), 2803 (w), 2783 (w), 2745 (w), 2475 (w), 2158 (w), 1603 (m), 1530 (m), 1512 (m), 1479 (w), 1443 (m), 1408 (m), 1393 (m), 1373 (m), 1314 (m), 1246 (m), 1233 (m), 1190 (m), 1165 (s), 1099 8 m), 1065 (m), 1020 (w), 976 (m), 949 (m), 866 (m), 839 (s), 820 (s), 791 (m), 760 (s), 739 (m), 704 (m), 687 (m), 664 (m), 650 (m), 629 cm^{-1} (m); ^1H NMR ($CDCl_3$, 300 MHz): δ = 0.22 (s, 9H), 3.00 (s, 6H), 6.68–6.74 (m, 2H), 8.04–8.11 ppm (m, 4H); ^{13}C NMR ($CDCl_3$, 75 MHz): δ = −0.4 (CH_3), 40.4 (CH_3), 102.9 (C_{quat}), 103.4 (C_{quat}), 111.4 (CH), 129.2 (C_{quat}), 129.6 (C_{quat}), 131.3 (C_{quat}), 133.6 (CH), 135.1 (CH), 138.2 (CH), 138.9 (CH), 140.0 (CH), 151.8 (CH), 155.2 ppm (CH); EI-MS: *m/z* (%): 415 (21) $[M]^+$(^{37}Cl), 414 (13), 413 (28) $[M]^+$(^{35}Cl), 322 (14), 141 (13), 129 (18), 111 ((^{37}Cl), 14), 109 ((^{35}Cl), 5), 97 (17) $[M(^{37}Cl)-Si(CH_3)_3]^+$, 95 (7) $[M(^{35}Cl)-Si(CH_3)_3]^+$, 85 ((^{37}Cl), 26), 83 ((^{35}Cl), 15), 71 ((^{35}Cl), 31), 69 ((^{37}Cl), 17), 57 ((^{37}Cl), 47), 55 ((^{35}Cl), 22) 43 ((^{37}Cl), 36), 41 ((^{35}Cl), 17); elemental analysis calcd (%) for $C_{21}H_{21}Cl_2N_3Si$ (415.0): C 54.11, H 3.74, N 7.42, S 8.50; found: C 54.40, H 3.95, N 7.20, S 8.20.

Acknowledgements

We cordially thank Fonds der Chemischen Industrie and Deutsche Forschungsgemeinschaft (Mu 1088/9-1) for the financial support. Computational support and infrastructure was provided by the "Centre for Information and Media Technology" (ZIM) at the University of Düsseldorf (Germany). We cordially thank Tobias Wilcke (Heinrich-Heine-Universität Düsseldorf) for taking the photograph for the graphical abstract.

Conflict of interest

The authors declare no conflict of interest.

Keywords: density functional calculations · fluorescence · heterocycles · multicomponent reactions · solvatochromism

[1] *Functional Organic Materials*; T. J. J. Müller, U. H. F. Bunz, eds.; Wiley-VHC, Weinheim, **2007**.
[2] S. R. Forrest, M. E. Thompson, *Chem. Rev.* **2007**, *107*, 923 – 924.
[3] For reviews on OFETs, see, for example: a) L. Torsi, M. Magliulo, K. Manoli, G. Palazzo, *Chem. Soc. Rev.* **2013**, *42*, 8612 – 8628; b) M. Mas-Torrent, C. Rovira, *Chem. Soc. Rev.* **2008**, *37*, 827 – 838; for reviews on OLEDs, see, for example: c) N. Thejo Kalyania, S. J. Dhoble, *Renewable Sustainable Energy Rev.* **2012**, *16*, 2696 – 2723; d) K. T. Kamtekar, A. P. Monkman, M. R. Bryce, *Adv. Mater.* **2010**, *22*, 572 – 582; for a review on DSSCs, see, for example: e) A. Hagfeldt, G. Boschloo, L. Sun, L. Kloo, H. Pettersson, *Chem. Rev.* **2010**, *110*, 6595 – 6663; f) N. Prabavathy, S. Shalini, R. Balasundaraprabhu, D. Velauthapillai, S. Prasanna, N. Muthukumarasamy, *Int. J. Energy Res.* **2017**, *41*, 1372 – 1396.
[4] a) G. S. Loving, M. Sainlos, B. Imperiali, *Trends Biotechnol.* **2010**, *28*, 73 – 83; b) Z. Zhang, Y. Zheng, Z. Sun, Z. Dai, Z. Tang, J. Ma, C. Maa, *Adv. Synth. Catal.* **2017**, *359*, 2259 – 2268.
[5] a) K. P. Carter, A. M. Young, A. E. Palmer, *Chem. Rev.* **2014**, *114*, 4564 – 4601; b) H. Kobayashi, M. Ogawa, R. Alford, P. L. Choyke, Y. Urano, *Chem. Rev.* **2010**, *110*, 2620 – 2640.
[6] A. P. Demchenko, Y. Mély, G. Duportail, A. S. Klymchenko, *Biophys. J.* **2009**, *96*, 3461 – 3470.
[7] A. Hantzsch, *Ber. Dtsch. Chem. Ges.* **1922**, *55*, 953 – 979.
[8] Z. R. Grabowski, K. Rotkiewicz, W. Rettig, *Chem. Rev.* **2003**, *103*, 3899 – 4031.
[9] a) M. D. Burke, S. L. Schreiber, *Angew. Chem. Int. Ed.* **2004**, *43*, 46 – 58; *Angew. Chem.* **2004**, *116*, 48 – 60; b) E. Ruijter, R. Scheffelaar, R. V. A. Orru, *Angew. Chem. Int. Ed.* **2011**, *50*, 6234 – 6346; *Angew. Chem.* **2011**, *123*, 6358 – 6371.
[10] T. J. J. Müller, in *Relative Reactivities of Functional Groups as the Key to Multicomponent Reactions in Multicomponent Reactions 1, Science of Synthesis* (Ed.: T. J. J. Müller), Thieme, Stuttgart, **2014**, pp. 5 – 27.
[11] a) T. J. J. Müller, D. M. D'Souza, *Pure Appl. Chem.* **2008**, *80*, 609 – 620; b) L. Levi, T. J. J. Müller, *Eur. J. Org. Chem.* **2016**, *2016*, 2902 – 2918.
[12] a) L. Levi, T. J. J. Müller, *Chem. Soc. Rev.* **2016**, *45*, 2825 – 2846; b) F. de Moliner, N. Kielland, R. Lavilla, M. Vendrell, *Angew. Chem. Int. Ed.* **2017**, *56*, 3758 – 3769; *Angew. Chem.* **2017**, *129*, 3812 – 3823; c) R. Riva, L. Moni, T. J. J. Müller in *Targets in Heterocyclic Systems, Vol. 20*, RSC, Cambridge, **2016**, pp. 85 – 112; d) T. J. J. Müller in *Aggregation Induced Emission: Materials and Applications* (Eds.: M. Fujiki, B. Z. Tang, B. Liu), ACS Symposium Series e-book, **2016**, Chapter 6, pp. 85 – 112.
[13] F. Yu, S.-C. Cui, X. Li, Y. Peng, Y. Yu, K. Yun, S.-C. Zhang, J. Li, J.-G. Liu, J. Hua, *Dyes Pigm.* **2017**, *139*, 7 – 18.
[14] K. R. Justin Thomas, M. Velusamy, J. T. Lin, C.-H. Chuen, Y.-T. Tao, *Chem. Mater.* **2005**, *17*, 1860 – 1866.
[15] L. Liu, G. Zhang, B. He, S. Liu, C. Duan, F. Huang, *Mater. Chem. Front.* **2017**, *1*, 499 – 506.
[16] K. Pei, Y. Wu, A. Islam, S. Zhu, L. Han, Z. Geng, W. Zhu, *J. Phys. Chem. C* **2014**, *118*, 16552 – 16561.
[17] J. Yuan, L. Qiu, Z. Zhang, Y. Li, Y. He, L. Jiang, Y. Zou, *Chem. Commun.* **2016**, *52*, 6881 – 6884.
[18] M. Eugenio Vázquez, J. B. Blanco, B. Imperiali, *J. Am. Chem. Soc.* **2005**, *127*, 1300 – 1306.
[19] L. E. Seitz, W. J. Suling, R. C. Reynolds, *J. Med. Chem.* **2002**, *45*, 5604 – 5606.
[20] C. Duan, F. Huang, Y. Cao, *J. Mater. Chem.* **2012**, *22*, 10416 – 10434.
[21] H. Hayashi, A. S. Touchy, Y. Kinjo, K. Kurotobi, Y. Toude, S. Ito, H. Saarenp, N. V. Tkachenko, H. Lemmetyinen, H. Imahori, *ChemSusChem* **2013**, *6*, 508 – 517.
[22] a) For a recent review on luminescent quinoxalines, see, for example: S. Achelle, C. Baudequin, N. Plé, *Dyes Pigm.* **2013**, *98*, 575 – 600; b) S. Achelle, A. Barsella, C. Baudequin, B. Caro, F. Robin-le Guen, *J. Org. Chem.* **2012**, *77*, 4087 – 4096; c) H. Wang, G. Chen, Y. Liu, I. Hu, X. Xu, S. Ji, *Dyes Pigm.* **2009**, *83*, 269 – 275; d) K. Justin Thomas, J. T. Lin, Y.-T. Tao, C.-H. Chuen, *Chem. Mater.* **2002**, *14*, 2796 – 2802.
[23] Y. Wu, W. Zhu, *Chem. Soc. Rev.* **2013**, *42*, 2039 – 2058.
[24] C. F. Gers-Panther, H. Fischer, J. Nordmann, T. Seiler, T. Behnke, C. Würth, W. Frank, U. Resch-Genger, T. J. J. Müller, *J. Org. Chem.* **2017**, *82*, 567 – 578.
[25] H. T. Black, I. Pelse, R. M. W. Wolfe, J. R. Reynolds, *Chem. Commun.* **2016**, *52*, 12877 – 12880.

[26] K. Kudo, A. Momotake, Y. Kanna, Y. Nishimura, T. Arai, *Chem. Commun.* **2011**, *47*, 3867 – 3869.
[27] K. Kudo, A. Momotake, J. K. Tanaka, Y. Miwa, T. Arai, *Photochem. Photobiol. Sci.* **2012**, *11*, 674 – 678.
[28] a) D. W. Chang, H. J. Lee, J. H. Kim, S. Y. Park, S. M. Park, L. Dai, J. B. Baek, *Org. Lett.* **2011**, *13*, 3880 – 3883; b) K. Pei, Y. Z. Wu, W. J. Wu, Q. Zhang, B. Q. Chen, H. Tian, W. H. Zhu, *Chem. Eur. J.* **2012**, *18*, 8190 – 8200.
[29] C. F. Gers, J. Nordmann, C. Kumru, W. Frank, T. J. J. Müller, *J. Org. Chem.* **2014**, *79*, 3296 – 3310.
[30] Z. Zhang, Z. Dai, X. Jiang, *Asian J. Org. Chem.* **2015**, *4*, 1370 – 1374.
[31] E. Merkul, J. Dohe, C. Gers, F. Rominger, T. J. J. Müller, *Angew. Chem. Int. Ed.* **2011**, *50*, 2966 – 2969; *Angew. Chem.* **2011**, *123*, 3023 – 3026.
[32] C. Boersch, E. Merkul, T. J. J. Müller, *Angew. Chem. Int. Ed.* **2011**, *50*, 10448 – 10452; *Angew. Chem.* **2011**, *123*, 10632 – 10636.
[33] E. Merkul, T. Oeser, T. J. J. Müller, *Chem. Eur. J.* **2009**, *15*, 5006 – 5011.
[34] a) O. Hinsberg, *Ber. Dtsch. Chem. Ges.* **1884**, *17*, 318 – 323; b) G. Körner, *Ber. Dtsch. Chem. Ges.* **1884**, *17*, A572 – A573.
[35] a) S. Gobec, U. Urleb, *Quinoxalines in Science of Synthesis* **2003**, *16*, 848 – 852; b) D. F. Saifina, N. A. Mamedov, *Russ. Chem. Rev.* **2010**, *79*, 351 – 370.
[36] M. Guo, D. Li, Z. Zhang, *J. Org. Chem.* **2003**, *68*, 10172 – 10174.
[37] Z. Zhang, X. Jiang, *Org. Lett.* **2014**, *16*, 4400 – 4403.
[38] A. Ianni, S. R. Waldvogel, *Synthesis* **2006**, *13*, 2103 – 2112.
[39] B. Unterhalt, P. Gores, *Arch. Pharm.* **1989**, *322*, 839 – 840.
[40] A. R. Katritzky, B. Galuszkag, S. Rachwalsand, D. Lynch, *Org. Prep. Proced.* **1993**, *25*, 557 – 562.
[41] I. T. Barnish, P. E. Cross, J. C. Danilewicz, R. P. Dickinson, D. A. Stopher, *J. Med. Chem.* **1981**, *24*, 399 – 404.
[42] CCDC1813052 (**4u**) contains the supplementary crystallographic data for this paper. These data are provided free of charge by The Cambridge Crystallographic Data Centre. See Table S5 in the Supporting Information for a summary of the X-ray structure data.
[43] a) X.-J. Yang, F. Drepper, B. Wu, W.-H. Sun, W. Haehnel, C. Janiak, *Dalton Trans.* **2005**, 256 – 267; b) C. Janiak, *J. Chem. Soc. Dalton Trans.* **2000**, 3885 – 3896.
[44] a) V. Lozan, P.-G. Lassahn, C. Zhang, B. Wu, C. Janiak, G. Rheinwald, H. Lang, *Z. Naturforsch. B* **2003**, *58*, 1152 – 1164; b) C. G. Zhang, C. Janiak, *Z. Anorg. Allg. Chem.* **2001**, *627*, 1972 – 1975; c) C. G. Zhang, C. Janiak, *J. Chem. Crystallogr.* **2001**, *31*, 29 – 35; d) H.-P. Wu, C. Janiak, G. Rheinwald, H. Lang, *J. Chem. Soc. Dalton Trans.* **1999**, 183 – 190; e) C. Janiak, L. Uehlin, H.-P. Wu, P. Klüfers, H. Piotrowski, T. G. Scharmann, *J. Chem. Soc. Dalton Trans.* **1999**, 3121 – 3131; f) H.-P. Wu, C. Janiak, L. Uehlin, P. Klüfers, P. Mayer, *Chem. Commun.* **1998**, 2637 – 2638.
[45] A. Ekbote, T. Jadhav, R. Misra, *New J. Chem.* **2017**, *41*, 9346 – 9353.
[46] S. Fery-Forgues, D. Lavabre, *J. Chem. Educ.* **1999**, *76*, 1260 – 1264.
[47] J. R. Lakowicz, *Principles of Fluorescence Spectroscopy*, 3rd ed.; Springer: Berlin/Heidelberg, **2006**; pp. 687 – 688.
[48] C. Hansch, A. Leo, R. W. Taft, *Chem. Rev.* **1991**, *91*, 165 – 195.
[49] J. R. Lakowicz, *Principles of Fluorescence Spectroscopy*, 3rd ed.; Springer: Berlin/Heidelberg, **2006**; pp. 213 – 216.
[50] a) Z. E. Lippert, *Ber. Bunsen-Ges.* **1957**, *61*, 962 – 975; b) N. Mataga, Y. Kaifu, M. Koizumi, *Bull. Chem. Soc. Jpn.* **1956**, *29*, 465 – 470.
[51] Gaussian 09, Revision A.02, M. J. Frisch, G. W. Trucks, H. B. Schlegel, G. E. Scuseria, M. A. Robb, J. R. Cheeseman, G. Scalmani, V. Barone, B. Mennucci, G. A. Petersson, H. Nakatsuji, M. Caricato, X. Li, H. P. Hratchian, A. F. Izmaylov, J. Bloino, G. Zheng, J. L. Sonnenberg, M. Hada, M. Ehara, K. Toyota, R. Fukuda, J. Hasegawa, M. Ishida, T. Nakajima, Y. Honda, O. Kitao, H. Nakai, T. Vreven, J. A. Montgomery, Jr., J. E. Peralta, F. Ogliaro, M. Bearpark, J. J. Heyd, E. Brothers, K. N. Kudin, V. N. Staroverov, R. Kobayashi, J. Normand, K. Raghavachari, A. Rendell, J. C. Burant, S. S. Iyengar, J. Tomasi, M. Cossi, N. Rega, J. M. Millam, M. Klene, J. E. Knox, J. B. Cross, V. Bakken, C. Adamo, J. Jaramillo, R. Gomperts, R. E. Stratmann, O. Yazyev, A. J. Austin, R. Cammi, C. Pomelli, J. W. Ochterski, R. L. Martin, K. Morokuma, V. G. Zakrzewski, G. A. Voth, P. Salvador, J. J. Dannenberg, S. Dapprich, A. D. Daniels, O. Farkas, J. B. Foresman, J. V. Ortiz, J. Cioslowski, D. J. Fox, Gaussian, Inc., Wallingford CT, **2009**.
[52] a) C. Lee, W. Yang, R. G. Parr, *Phys. Rev. B: Condens. Matter Mater. Phys.* **1988**, *37*, 785 – 789; b) A. D. Becke, *J. Chem. Phys.* **1993**, *98*, 1372 – 1377; c) K. Kim, K. D. Jordan, *J. Phys. Chem.* **1994**, *98*, 10089 – 10094; d) P. J. Stephens, F. J. Devlin, C. F. Chabalowski, M. J. Frisch, *J. Phys. Chem.* **1994**, *98*, 11623 – 11627.
[53] R. Krishnan, J. S. Binkley, R. Seeger, J. A. Pople, *J. Chem. Phys.* **1980**, *72*, 650 – 654.
[54] G. Scalmani, M. J. Frisch, *J. Chem. Phys.* **2010**, *132*, 114110.

Manuscript received: January 8, 2018
Accepted manuscript online: February 9, 2018
Version of record online: March 30, 2018